International Journal of Multiphase Flow 137 (2021) 103579

Contents lists available at ScienceDirect

International Journal of Multiphase Flow

journal homepage: www.elsevier.com/locate/ijmulflow

Experimental study of submerged hydraulic jumps generated downstream of rectangular plunging jets

José M. Carrillo*, Francisca Marco, Luis G. Castillo, Juan T. García

Escuela Técnica Superior de Ingeniería de Caminos, Canales y Puertos e Ingeniería de Minas, Universidad Politécnica de Cartagena, Paseo Alfonso XIII, 52 - 30203 Cartagena, Spain

ARTICLE INFO

Article history:
Received 10 June 2020
Revised 11 January 2021
Accepted 23 January 2021
Available online 27 January 2021

Keywords:
Air-water flow
Back-flushing Pitot tube
Falling jet
Optical fiber probe
Overtopping
Submerged hydraulic jump

ABSTRACT

This experimental study analyzes submerged hydraulic jumps generated in a 1.05-m wide stilling basin that receives overflow rectangular impinging jets, with the vertical distance between the sharp-crested weir and the bottom of the plunge pool being 2.20 m. Five submerged hydraulic jumps downstream of non-developed nappe jets were analyzed, with vertical falling distances to break-up length ratios between 0.76 and 0.78. The impingement velocity range was from 6.12 to 6.33 m/s, while the water depth / impingement jet thickness ratios were between 8.45 and 15.00. The velocity field and air entrapped were measured in several cross sections, with the farthest sections being located 1.0 m from the stagnation point. The entrapped air (void fraction and phase change detection) behavior measured with a phase-detection probe was classified as a function of the distance to the stagnation point / impingement jet thickness ratio and/or the mean void fraction of the vertical profiles. The maximum void fractions were observed near the free surface. However, the higher phase change detection frequencies (up to 130-140 Hz) were obtained near the bottom for local void fractions smaller than 0.15-0.20. The non-dimensional velocity distribution seems to be similar to previous published studies, extending their validity range. Furthermore, the free hydraulic jumps formula has been adapted to estimate the air rate in the shear stress layer and the growth of the characteristic length in the plunge pool.

1. Introduction

In recent decades, improvements in the knowledge of the time-series and changes in dam safety regulations have made it necessary to re-evaluate the spillways and outlets capacity of large dams, and their operational scenarios around the world. Several studies (e.g., FEMA, 2013, 2014) have demonstrated that many weirs may have an insufficient flow discharge capacity, thereby increasing the possibility of being overtopped in extreme events. During extreme conditions, the overflow may be considered as an additional operational strategy, although at the risk of raising new hydrodynamic scenarios for the dams that may cause local erosion and scour at the toe of the dam.

The type of stilling basin is a technical-economic choice between a lined shallow plunge pool or an unprotected deep plunge pool. For safety operations, the designers require data regarding the magnitude and frequency of the hydrodynamic actions at the bottom of the plunge pool. The impingement jet characteristics and the water cushion depths define the bottom requirements to resist scour at the toe of the dam (Annandale, 2006).

Several studies have focused on the air entrainment, free surface perturbations and break-up length of turbulent jets (e.g., Horeni, 1956; Ervine and Falvey, 1987; Ervine et al., 1997; Castillo, 2006). In addition, the characteristics of the near region flow of turbulent jets entering water cushions have been studied by several authors (e.g., Albertson et al., 1950; Ervine and Falvey, 1987; Ervine et al., 1997; Bollaert and Schleiss, 2003; Chanson et al., 2004; Manso et al., 2007; Bertola et al., 2018; Xu et al., 2018).

A better understanding of the flow pattern in submerged hydraulic jumps of plunge pools is essential for the designers as it may affect their designs. The entrapped air in the plunge pool may play an important role in hydraulic structure safety operations. This creates a great increment in the flow depth of the mixture. The entrained air may also affect the behavior of the stilling basin, influencing the characteristics of the vortices. According to Duarte et al. (2015), two opposing effects may be generated

* Corresponding author.
E-mail address: jose.carrillo@upct.es (J.M. Carrillo).

https://doi.org/10.1016/j.ijmultiphaseflow.2021.103579

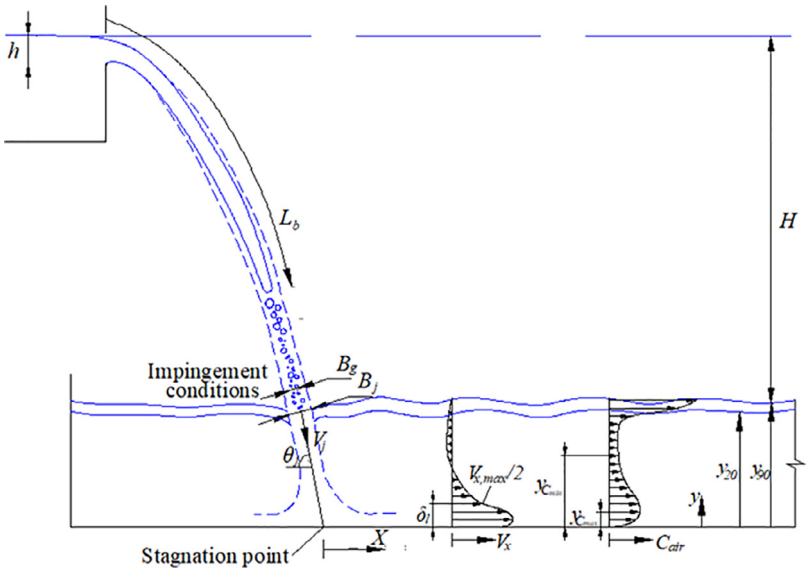

Fig. 1. Definition sketch of a submerged hydraulic jump downstream of a nappe jet.

by air entrainment. Due to its lower apparent density, aerated jets have lower momentum than similar clear water jets, contributing to having lower pressures on the bottom of the plunge pool. However, the air bubbles lower the shear stresses in the pool, allowing the aerated jets to flow with a higher velocity. The influence of air entrainment is a balance between these two effects.

A hydraulic jump is a local non-uniform transition from supercritical to subcritical flow regime. The hydraulic jump is a discontinuity in the free surface characterized by a steep upward slope, the development of eddies at different scales, surface waves and undulation of the free surface, spray, energy dissipation and large amounts of air entrainment. Due to their high energy dissipation, they may be designed as energy dissipaters, whose efficiency is directly related to the supercritical Froude number. A review of the general knowledge in free hydraulic jumps and equipment to measure the flow properties may be found in Valero et al. (2018).

According to Wood (1991), the void fraction is one of the key parameters to be analyzed in hydraulic jumps. The entrained air in stilling basins may affect the behavior and the safety operation of hydraulic structures (e.g., to protect hydraulic structures from cavitation damage, to design the required wall elevation of the stilling basin to avoid overflows due to bulking and/or undulations of the free surface, among others).

In free hydraulic jumps, the air enters mainly at the jump toe into a free shear layer, characterized by intensive turbulence production, predominantly in vortices with axes perpendicular to the flow direction. A better knowledge of mixing, diffusion, transfer processes and air/water gas exchanges depends on the ability to measure these two-phase turbulent flows (Murzyn, 2010).

When the tailwater level is higher than the conjugated or sequent water depth, for the same inlet Froude number, the hydraulic jump is drowned out. In submerged hydraulic jumps generated downstream of gates, the air entrainment and the turbulence intensities are smaller than for their free jump counterparts (Rajaratnam, 1965), as well as showing relatively gentle surface profiles (Long et al., 1991). Long et al. (1990) considered that submerged hydraulic jumps may be treated as a transition between free hydraulic jumps and wall jets, and may be treated as wall jets under an adverse pressure gradient. The authors also distinguished three regions in submerged hydraulic jumps: the developing, the fully developed, and the recovering regions. Later, Peiqing et al. (1998) distinguished three regions in the main flow direction of plunge pools: region I located between the impingement point of the free falling jet and the distance from the bottom where its influence does not affect the characteristics of the submerged jet; region II located near the stagnation point, where the flow experiences such considerable deflection that the velocities decrease rapidly and the pressures increase sharply; region III in which the flow behavior is similar to that of a submerged wall jet, the main flow diffuses rapidly along the bottom of the plunge pool and a large recirculating region is formed at the surface.

Fig. 1 shows a sketch of a submerged hydraulic jump generated in a plunge pool. The figure includes the velocity and air concentration distributions based on the results obtained and the observations made by several authors in hydraulic jumps.

With regard to the plunge pool aeration, there are at least three main mechanisms as reported by Ervine (1998). The first mechanism considers the surface disturbances of the falling jet on the aeration process, with the minimum jet velocity to entrain air depending on the jet turbulence level (Ervine et al., 1980). In the second mechanism, a thin air boundary layer is dragged along by the jet; the air flow may be able to enter the receiving water when a gap is formed between the jet and the recirculating flow. This second mechanism is usually only thought to be significant for jet velocities beyond 5 m/s. The third mechanism is a free-surface aeration which contributes to the overall aeration rate. This can be present in the falling jet, particularly at high velocities ($>$ 6 m/s), and can also occur due to the violent disturbances on the surface of the plunge pool.

Using phase detection probes, several studies have focused on the void fraction or air concentration analysis in free hydraulic jumps (e.g., Chanson, 1995; Murzyn and Chanson, 2007; 2009; Murzyn, 2010). Two different regions may be distinguished: an air-water shear layer near the bottom, characterized by smaller bubble sizes (typically in millimeters) and high air content, and a recirculation region located in the upper part of the vertical profiles. A strong unsteady recirculation appears in the second region, with bubbles of different sizes, and the presence of air-water packets. Near the free surface, a foam structure layer may be observed. To the best of our knowledge, the current understanding of two-phase flows in the submerged hydraulic jump of free falling rectangular jets is scarce (e.g., Castillo et al., 2017; Carrillo et al., 2020a). The present work aims to improve the studies in the far field of the plunge pool (namely fully developed submerged wall jet region).

Fig. 2. Detail of the plunge pool in the experimental facility with the optical fiber probe.

This study experimentally analyzes submerged hydraulic jumps generated downstream of rectangular falling jets, with falling distances from the weir crest to the bottom of the plunge pool of 2.20 m. An optical fiber probe and a back-flushing Pitot tube have been employed to analyze the entrapped air and the velocity field, respectively. Void fraction rates, free surface undulation pattern, phase-change detection frequency, mean velocities near the bottom, and Sauter mean bubble diameter have been analyzed in the submerged hydraulic jumps generated downstream of the stagnation point of rectangular free falling jets.

2. Materials and methods

2.1. Experimental setup

The experiments were conducted in an experimental facility located in the Hydraulic Laboratory of the Universidad Politécnica de Cartagena (Spain). The relatively large infrastructure may be divided into two parts:

A 4.00 m long and 1.05 m wide inlet channel that ends in a 0.85 m rectangular sharp-crested weir with a weir height of 0.325 m. The channel has a labyrinth to increase the flow trajectory, two gravel filters and a 0.30 m honeycomb panel for dissipating energy and straightening the streamlines before the weir. The weir crest elevation was located at vertical distance $P_l = 2.20$ m from the bottom of the stilling basin.

A 1.05 m wide, 3.00 m long, and 1.60 m high stilling basin, built in methacrylate (Fig. 2). The plunge pool enables different water cushion depths to be analyzed by modifying the height of the wall located in the downstream side. Further information on the experimental device is available in Carrillo (2014).

The flows were measured with an Endress + Hauser electromagnetic flowmeter installed in the supply line. The device had an accuracy of ±0.5%. The upstream energy head over the sharp-crested weir was estimated with a point gauge, with an accuracy of ±0.5 mm.

An optical fiber probe and a modified Pitot tube were used to measure the entrapped air and the velocity field in the centerline of the stilling basin. The submerged hydraulic jumps generated downstream of the stagnation point of the impingement jets were measured in ten cross sections, spaced 0.10 m apart. The stagnation point was considered by using the trajectory of the central nappe proposed by Scimemi (1930). According to our previous findings, this expression seems to be a good estimator of the maximum pressure distribution point measured on the bottom of the plunge pool, with differences of ±1 cm for $q > 0.037$ m^3/s/m (Carrillo, 2014; Castillo et al., 2014). In each section, the vertical profile was measured. The probes were mounted on a trolley that enabled longitudinal, transversal and vertical displacements. The desired location in the three directions was measured by rules, with an estimated accuracy of ±1 mm.

The flow conditions were selected to analyze non-developed jets (vertical distance between the energy head over the weir crest and at the end of the plunge pool to the break-up length ratio $H/L_b < 1.0$), and effective water cushion depths (water depth at the end of the plunge pool to impingement jet thickness ratio $Y/B_j > 5.5$ according to Castillo et al., 2015). To facilitate the analysis of the water cushion ratio influence (Y/B_j from 8.45 to 15.00), the cases selected had a similar impingement jet velocity, H/L_b ratio and angle of the impingement jet θ_j, estimated by the Scimemi (1930) formula, and mean void fraction at the impingement condition $C_{mean,\,j}$.

Five different submerged hydraulic jumps were studied in the stilling basin, with specific flow rates q from 0.099 to 0.073 m^3/s/m, and equivalent impingement Froude number F_r^*, that is, calculated with gravitational jet thickness B_g and gravitational velocity V_j, from 15.51 to 17.13. The gravitational data were obtained with the Bernoulli formula, neglecting energy losses and without considering air entrainment. Tables 1 and 2 summarize some of the most representative parameters in rectangular free falling jets, where h is the energy head over the weir crest, and R_e and W_e are, respectively, the Reynolds and Weber numbers obtained upstream of the sharp-crested weir.

Table 1
Experimental flow conditions: dimensional parameters.

q(m^3/s/m)	h(m)	H(m)	Y(m)	V_j(m/s)	B_g(m)	B_j(m)	L_b(m)	θ_j(°)
0.099	0.144	2.044	0.290	6.33	0.017	0.034	2.69	78.4
0.089	0.135	2.001	0.324	6.26	0.016	0.032	2.61	78.7
0.085	0.130	1.979	0.341	6.23	0.015	0.030	2.57	78.9
0.079	0.124	1.938	0.376	6.16	0.014	0.028	2.51	79.0
0.073	0.118	1.907	0.401	6.11	0.013	0.027	2.45	79.2

Table 2
Experimental flow conditions: non-dimensional parameters.

q(m^3/s/m)	Y/B_j(-)	H/L_b(-)	$C_{mean,\,j}$(-)	F_r^*(-)	R_e(-)	W_e(-)	$R_e^{\,0.2}W_e^{0.6}$(-)
0.099	8.45	0.76	0.54	15.50	161463	2794	1286
0.089	10.25	0.77	0.55	15.80	146565	2456	1168
0.085	11.28	0.77	0.55	16.24	138498	2277	1103
0.079	13.20	0.77	0.54	16.62	129021	2072	1028
0.073	15.00	0.78	0.56	17.11	119771	1876	954

Following Castillo (2006) and Castillo et al. (2015), the impingement jet thickness was estimated as:

$$B_j = B_g + 2\xi = \frac{q}{\sqrt{2gH}} + 4\varphi\sqrt{h}\left(\sqrt{2H} - 2\sqrt{h}\right) \quad (1)$$

where ξ is the lateral jet spread thickness due to the turbulence effect and $\varphi = K_\varphi T_u$, with T_u being the turbulence intensity and $K_\varphi = 1.24$ for nappe flow case.

The break-up length L_b defines the distance from where the jet becomes fully developed, which means that the non-aerated jet core disappears (see L_b in Fig. 1). It was calculated as per (Castillo et al., 2015):

$$\frac{L_b}{B_i F_i^2} = \frac{K}{\left(K_\varphi T_u F_i^2\right)^{0.82}} \quad (2)$$

with B_i, F_i and T_u being the jet thickness, the Froude Number, and the turbulent intensity at the issuance conditions, respectively, and $K \approx 0.85$ a dimensionless coefficient.

For prototype specific flows ($q >> 0.25$ m^3/s/m), a mean turbulence index $T_u \sim 1.2\%$ may be considered (Castillo, 2006). However, for laboratory specific flow ($q < 0.25$ m^3/s/m), the turbulence intensity at issuance conditions may be estimated as (Castillo et al., 2015):

$$T_u^* = \frac{q^{0.43}}{IC} \quad (3)$$

$$IC = \frac{14.95 g^{0.50}}{K^{1.22} C_d^{0.19}} \quad (4)$$

with IC being the initial conditions, g the gravitational acceleration, and C_d the discharge coefficient.

Possible scale effects may affect the initial conditions of the jet in the weir. To reduce the scale effects in rectangular weirs, Ranga Raju and Asawa (1977) estimated that the effects of viscosity and surface tension vanish for $R_e^{0.2}W_e^{0.6} > 900$ or head of 11.0 cm for water at 20 °C, in which $R_e = \sqrt{gh^3}/\nu$ and $W_e = \rho g h^2/\sigma$ are the Reynolds and Weber numbers, and ν, ρ and σ are the kinematic viscosity, the water density and the surface tension of the water, respectively.

Although the values shown in Tables 1 and 2 fulfil the recommendations of Ranga Raju and Asawa (1977), the air bubble size is not correctly scalable. For that reason, the air-water flow phenomenon must be scaled with particular caution (Chanson, 2009).

2.2. Optical fiber probe

To register the local void fraction, an RBI-Instruments phase detection change device was used. The equipment consisted of an optical probe that ends in a Descartes' prism. Considering that the water and the air have different refraction indexes, 1.33 and 1.00, respectively, the intensity of the reflected light may be related by the Fresnel formula. An optoelectronic module measures the light intensity reflected or diffracted by the prism depending on the fluid in contact with the prism and converts the signal into voltage. The rise and fall of the voltage are the arrival and departure of the phase change at the sensor tip, respectively. Thus, optical fiber equipment can be used to estimate the local phase change of the air-water mixture (RBI-Instruments, 2012).

Murzyn et al. (2005) considered that the minimum bubble sized detected by the device may be in the order of the optical fiber diameter (40 μm) in slow moving flows. However, the smallest size becomes a function of the signal sampling frequency (10^6 Hz) at high velocities.

Stutz and Reboud (1997a, 1997b) found that the relative uncertainty of the void fraction measured with optical probes can be estimated at approximately 15% of the measured value, and the sensitivity to a threshold variation is less than 1%.

For an accurate estimation of the air entrapped in the flow, the statistical count of the number of air bubbles in contact with the tips of the probe should be considered (Stutz, 1996). Hence, it is necessary to have large enough measurements for accurate results. In a study of stepped spillways, Boes and Hager (2003) consider that the accuracy of the void fraction in air-water flows is related to the variation of the air-water phase, instead of the sample duration t. Moreover, in stepped spillways, André et al. (2005) performed a sensitivity analysis of the probe behavior to test the minimum duration of their registers. The authors consider that measurements of 60 s may be considered a good balance between the duration of the sampling sequence and accuracy in order to obtain quasi-stationary values that are statistically representative of the void fraction. To err on the side of caution, previous studies in submerged hydraulic jumps have considered a sample time of 90 s (Carrillo et al., 2020b), obtaining a relative uncertainty of less than 1% of the mean value of the void fraction in this type of tests.

Ervine et al. (1997) proposed that the dominant frequencies in plunge pools may divide into two cases related with the impingement jet velocity V_j. The lowest frequencies are linked with large scale eddies with dimensions in the order of the plunge pool depth. Those frequencies are characterized by a recirculating velocity $V_r \approx 0.035\ V_j$, and a Strouhal number of the dominant eddies $S = fY/V_j \approx 0.01$, where f is the dominant fluctuation frequency. The eddy sizes contained with half of the shear layer width are characterized by the Strouhal number in the shear layer $S_s = f_s Y/V_j \approx 0.25$.

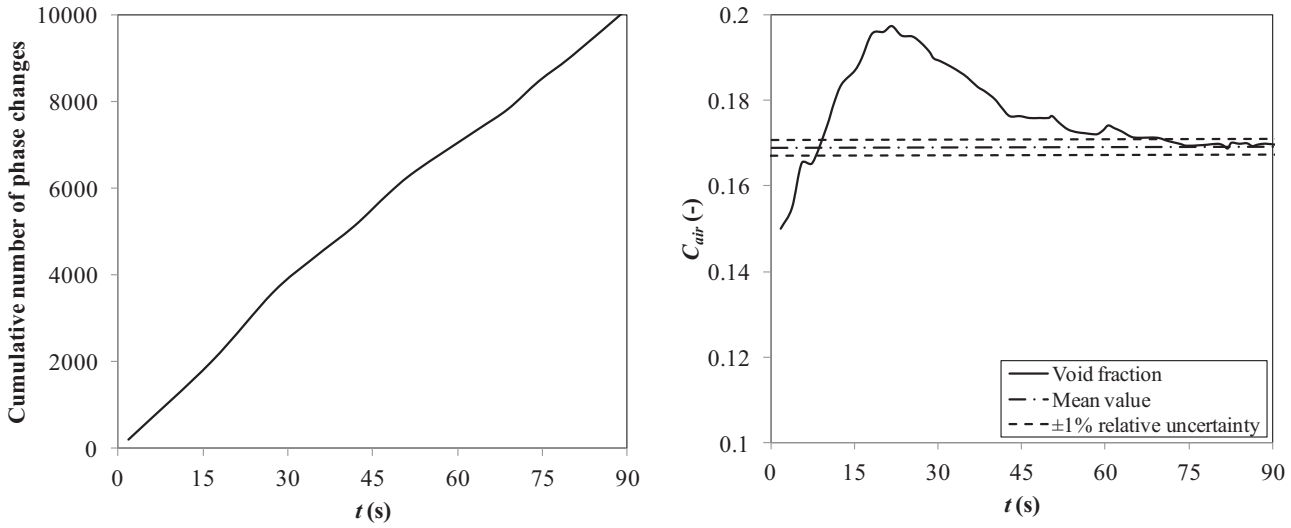

Fig. 3. Evolution of the phase changes and the air concentration measured by the optical fiber probe during a test.

Fig. 3 shows that, although the phase change detection frequency does not seem to be affected by the sample time (the slope of the cumulative number of phase changes is similar throughout the entire register), more than 60 s seem to be necessary to obtain a relative uncertainly below 1% in the void fraction measurements.

Taking those ideas into account, the far field downstream of the impingement jet point of the stilling basin was analyzed. A sample duration of 90 s was set in all the experimental campaign to reduce the relative uncertainty of the measurements, considering the expected large-scale eddies in the plunge pool. The statistically representative values of the void fraction were validated through repeatability tests.

Measurements were obtained with the probe located perpendicular to the bottom. In the vertical position, the sensitive tip forms a 45° angle with the horizontal and it was oriented to the upstream side. This design may reduce the bias effect in three-dimensional flow structures when only one tip is being used. According to Boes and Hager (1998), the size of the probe tip is rather small, so that it allows the measurement of tiny bubbles of about the probe tip diameter and the disturbance to the flow is small. However, as the flow may not be oriented in a single direction in a hydraulic jump, this equipment was used only to measure void fractions. A vertical definition of 0.0067 m was used near the bottom and near the free surface to capture the wall jet and the free surface undulation. In the middle part of the vertical profiles, the vertical resolution was incremented up to 0.020 m. In total, more than 1600 points were obtained with the optical probe device. These results allowed several parameters to be obtained: the local void fraction C_{air}, the phase change detection frequency F, and the water depths where the local void fraction was 90% (y_{90}), among others.

2.3. Back-flushing pitot tube

The time-averaged velocity field was measured by a modified Pitot tube to avoid air entrainment in the pipelines. The tip of the tube was positioned in the same positions as the optical fiber in the stilling basin. The Pitot tube has a diameter hole of 2.3 mm to measure the total pressure head at the tip of the tube, and a ring of ports located in the circumference of the tube to obtain the static pressure head. The external diameter of the Pitot tube is 12 mm. Total and static pressure heads were recorded with GE Druck model UNIK 5000 pressure sensors, with a measuring range between -200 and +800 mbar and an accuracy of ±0.04% of their full scale. The accuracy of the instantaneous pressure data was ±0.01 m after the static calibration. Signals were recorded for 90 s at 20 Hz.

To avoid the entrainment of air into the pneumatic pipelines of the Pitot tube, a back-flushing system was mounted. Following Matos and Frizell (2000) and Matos et al. (2002), the back-flushing was forced by a reservoir of constant head which fed both the total and the static pressure ports. Needle valves were used to control the back-flushing flow. To reduce the perturbation of the measurements by the back-flushing system, the flow rate was limited to almost zero.

Wood (1983) considered the following expression to obtain the mean velocity from the back-flushing Pitot tube in air-water flow conditions:

$$V = \sqrt{\frac{2g\Delta P}{\rho_w(1-\lambda C_{air})}} \tag{5}$$

where V is the time-averaged velocity, g the gravitational acceleration, ΔP the difference between the total pressure head and the static pressure head, ρ_w the water density, C_{air} the local void fraction, and λ the tapping coefficient which accounts for the non-homogeneous behavior of the air-water flow near the stagnation point of the Pitot tube.

Considering that the recirculation and backward flow may affect the measurements of the Pitot tube (Matos and Frizell, 2000; Matos et al., 2002), the local mean velocity analysis was limited to the wall jet region near the bottom of the plunge pool.

3. Results and discussion

3.1. Void fraction in the plunge pool

The local void fraction C_{air} may be estimated with phase change equipment relating the sum of the time the probe tip is in air (Σ_{tGi}) and the total time duration t of the measurement. An optical fiber probe was used to obtain the void fraction profiles in submerged hydraulic jumps of nappe jets. In each submerged hydraulic jump, cross sections from $X = 0.10$ m to 1.00 m were analyzed. At least 30 points were measured per cross section, obtaining more than 1600 registers.

Data of the different cross sections have been classified as a function of two different dimensionless parameters: the X/B_j ratio, with X being the distance of the vertical profile to the stagnation

Table 3
Minimum and maximum values of X/B_j and C_{mean} per submerged hydraulic jump.

q(m^3/s/m)	Y/B_j(-)	H/L_b(-)	$X/B_{j,\ min}$(-)	$X/B_{j,\ max}$(-)	$C_{mean\ min}$(-)	$C_{mean,\ max}$(-)
0.099	8.45	0.76	2.9	29.4	0.17	0.24
0.089	10.25	0.77	3.1	31.3	0.12	0.21
0.085	11.28	0.77	3.6	35.7	0.09	0.20
0.079	13.20	0.77	3.6	35.7	0.09	0.20
0.073	15.00	0.78	3.7	37.0	0.08	0.20

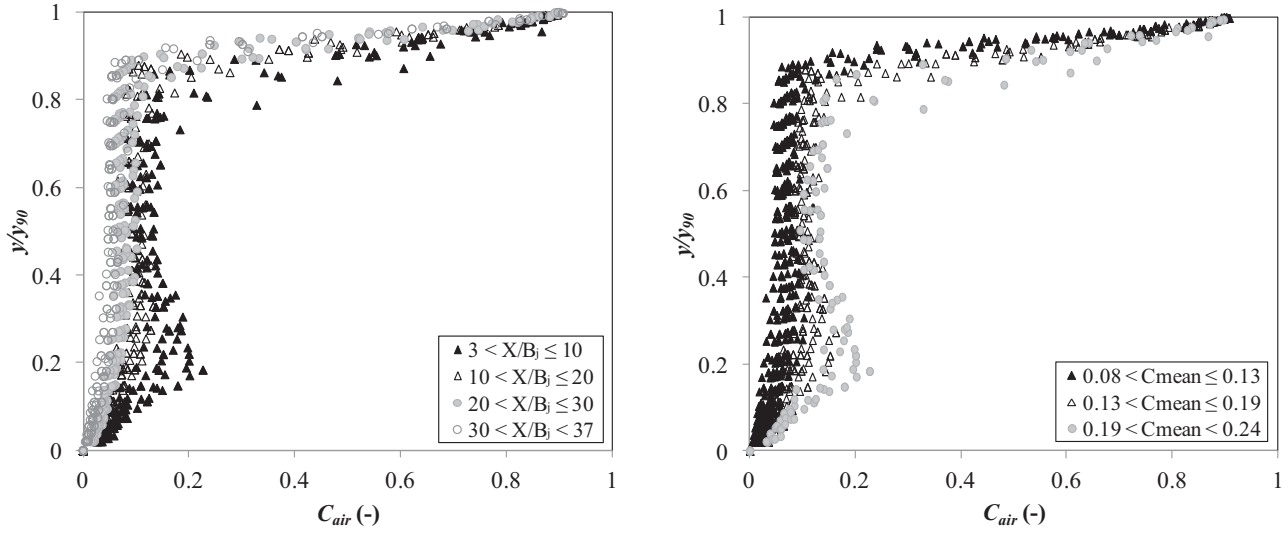

Fig. 4. Local void fraction profiles in the plunge pool.

point and B_j the impingement jet thickness, and the average concentration C_{mean} in each cross section, defined as:

$$C_{mean} = \frac{1}{y_{90}} \int_0^{y90} C_{air} dy \tag{6}$$

where y_{90} is the vertical distance from the bottom at which $C_{air} = 90\%$.

Table 3 details the range of the X/B_j ratio and the C_{mean} obtained per submerged hydraulic jump. Regarding the X/B_j ratio, all the flow conditions have vertical profiles between 3-4 and 30. However, the highest specific flow, with the biggest impingement jet thickness, has the smallest maximum X/B_j ratio. The C_{mean} extreme values obtained in each submerged hydraulic jump show greater variability, with few overlaps between the higher specific flow (with the smaller Y/B_j ratio), and the other specific flows.

Fig. 4 shows the void fraction profiles ($C_{air} = \Sigma_{tGi}/t$) of the five submerged hydraulic jumps analyzed. The y-axis has been normalized by the y_{90} value. The data have been grouped into four subclasses as a function of the X/B_j ratio. Different behaviors may be considered in the vertical profiles. All the profiles show their minimum values of C_{air} near the bottom ($y/y_{90} < 0.10$). The vertical profiles closer to the stagnation point show a first maximum peak around $0.15 < y/y_{90} < 0.30$, with the largest void fractions reaching values of around 20-25%. Those local peaks seem to be related with the air bubbles and the air pockets entrapment mechanisms observed by Ervine (1998). As Chanson (1995) reported, these air pockets are broken up into very thin air bubbles as they are entrained in the turbulent shear region, characterized by large air content. As the flow moves downstream from the stagnation point, the bubbles are diffused into regions of lower shear stresses, and the maximum peak of void fraction detected near the bottom tends to decrease. For $0.40 < y/y_{90} < 0.70$, the C_{air} value tends to a constant value in the vertical ($dC_{air}/(y/y_{90}) \approx 0$), that reduces from 8-13% to 5-7% as the distance from the stagnation point increases. Near the free surface ($y/y_{90} >$ 0.75-0.80), the air entrapped values tend to increase rapidly from 0.15-0.20 to 0.9. This may indicate the unsteady flow depth generated by intense turbulence and vorticity in the receiving pool as Ervine (1998) suggested.

The data can also be classified by considering the mean void fraction in the vertical profile. Fig. 4 also shows the void fraction data in a dimensionless way as a function of the average concentration in the vertical. Three different sub-classes can be identified. The vertical profiles with the maximum C_{mean} values (from 0.19 to 0.24) show a first maximum peak near to the bottom (around $0.15 < y/y_{90} < 0.30$), with the largest void fraction values reaching around 20-25%. This sub-class was mainly obtained with the cross sections measured by the maximum specific flow and the minimum water depth, and for the cross sections located closer to the stagnation point in the other specific flows (see the C_{mean} range in Table 3). The maximum peak near the bottom is not detected by the optical probe equipment in the other sub-classes. The data located at greater X/B_j ratios from the stagnation point tend to coincide with the smaller C_{mean} values (see Fig. 4). For $0.20 < y/y_{90} < 0.80$ (for $0.30 < y/y_{90} < 0.70$ in the maximum C_{mean} values sub-class), the C_{air} value tends to a constant value in the vertical that reduces from 8-13% to 5-7% as the average concentration decreases. Near the free surface, the void fraction increases rapidly independently of the sub-class.

Taking into account the analytical distribution of void fraction considered by Chanson and Brattberg (2000) and by Murzyn and Chanson (2009) in the air-water shear layer of free hydraulic jumps, the formula can be adapted to analyze the distribution of the void fraction measured near the stagnation point in the submerged hydraulic jumps as:

$$C_{air} = C_{max} e^{\left(-\frac{\left(\left(y-y_{C_{max}}\right)/B_j\right)^2}{4D^*\left(X/B_j\right)}\right)} \text{ valid for } y < y_{C_{min}} \tag{7}$$

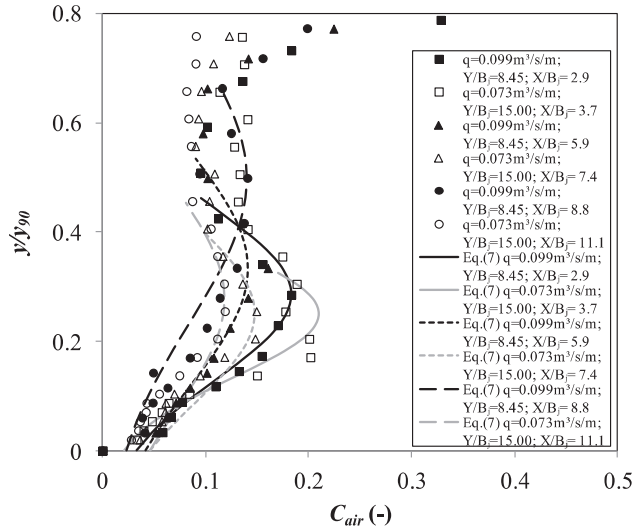

Fig. 5. Vertical distribution of void fraction at the beginning of the submerged hydraulic jump for the minimum and maximum specific flows.

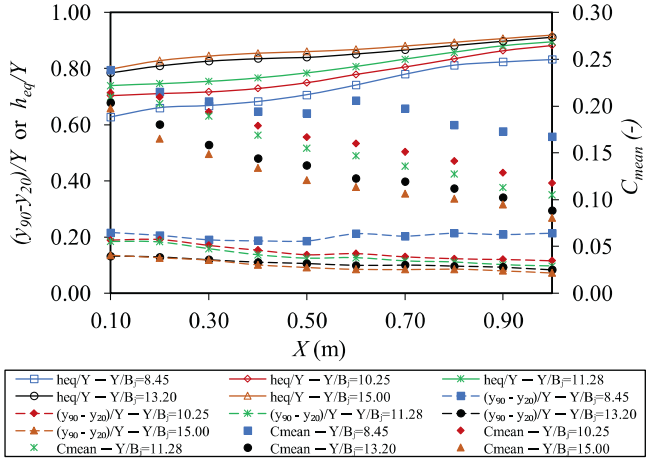

Fig. 6. Variation of the free surface undulation pattern and mean void fraction.

where C_{max} is the maximum void fraction in the shear layer, $Y_{C\,max}$ the vertical distance from the bottom to the maximum void fraction C_{max}, D^* a dimensionless turbulent diffusivity, and $y_{C_{min}}$ the vertical distance from the bottom to the local minimum void fraction at the boundary between the turbulent shear flow and the recirculation regions (see Fig. 1).

The dimensionless diffusivity $D^* = D_t/(V_j B_j)$, with D_t being the turbulent diffusivity assumed constant at a given longitudinal position, and V_j and B_j are the jet thickness and velocity at the impingement point, respectively. D^* deduced from best-fit data per vertical profile, ranged from 0.2 to 0.4, was in the order of that reported by Bertola et al. (2018) for a similar impingement Reynolds number in planar plunging water jets, tending to increase as the impingement Reynolds number tends to reduce.

Fig. 5 shows the detail of the shear stress layer measured with the minimum and maximum specific flows (q = 0.099 m^3/s/m, Y/B_j = 8.45, and q = 0.073 m^3/s/m, Y/B_j = 15.00, respectively) in the cross sections located between 0.10 and 0.30 m from the stagnation point. Although the formula proposed by Murzyn and Chanson (2009) was obtained for partially-developed hydraulic jumps downstream of a gate, the adjustments show reasonably good agreement once Eq. (7) has been modified for rectangular impingement jets.

3.2. Free surface undulation pattern

The water surface along a submerged hydraulic fluctuates, and the free surface is usually treated as an averaged depth profile (Long et al., 1990). Another recurrent treatment of the free surface in air-water flows is to use the equivalent water height h_{eq}, defined as the equivalent water depth that there would be in the absence of entrained air. In each cross section, the equivalent water height can be obtained as:

$$h_{eq} = (1 - C_{mean}) y_{90} \quad (8)$$

Fig. 6 shows the equivalent water depth, h_{eq}, as a function of Y, with Y being the y_{90} value at cross section X = 1.0 m of their corresponding submerged hydraulic jumps, and the mean void fraction C_{mean} along the plunge pool. In general, all the C_{mean} values tend to decrease as the X distance increases from the stagnation point, while the h_{eq}/Y ratio tends to increase, from 0.63-0.80 near the impingement point to 0.83-0.92 at X = 1.0 m. Those values confirm the expected reductions in mean air concentration and mean flow velocity as the cross sections are located further away from the impingement point.

Several studies (e.g., Lopes, 2011; Carrillo et al., 2019) analyzed the variation of the unsteady flow depth at a given location with conductivity probe measurements. Following the same approach, Fig. 6 also shows the $(y_{90}\text{-}y_{20})/Y$ ratio, with y_{20} being the vertical distance from the bottom at which C_{air} = 20%. The y_{20} value was selected taking into account the smaller void fraction above the $dC_{air}/(y/y_{90}) \approx 0$ region observed in Fig. 4, in which all the void fraction profiles show $C_{air} \leq 0.20$, occurring for y/y_{90} ratios between 0.4 and 0.7. Taking the sharper change in $dC_{air}/(y/y_{90})$into account, the $(y_{90}\text{-}y_{20})/Y$ ratio was considered as an estimator to analyze the free surface undulation in the plunge pool. In general, the distance between y_{20} and y_{90} tends to decrease slightly as the flow moves downstream. This indicates that there is a small reduction in the free surface undulation, namely waves, along the stilling basin that seems to be somehow related to the C_{mean} reduction. The results registered with the higher specific flow and the smaller water cushion depth (Y/B_j = 8.45 case) tend to obtain a constant $(y_{90}\text{-}y_{20})/Y$ ratio around 0.20 along the different cross sections. This different behavior seems to be related with the smaller submergence ratio of this hydraulic jump.

3.3. Phase change frequency

Several authors (e.g., Murzyn et al., 2005; Murzyn and Chanson, 2007) have analyzed the phase change detection frequency F in free hydraulic jumps. However, there are few references to submerged hydraulic jumps downstream of rectangular impingements free falling jets flows.

Fig. 7 shows the phase change frequency detected by the optical probe as a function of the X/B_j ratio. The sub-classes identified in the previous section can be used to define different behaviors. The local bubble count rate has been plotted in a dimensionless way, enabling comparison with those distributions previously obtained by several authors in free hydraulic jumps (e.g., Chanson and Brattberg, 2000; Murzyn et al., 2005; Chachereau and Chanson, 2011; Chanson and Chachereau, 2013). As those authors indicated, the maximum change detection frequency may be linked with the large turbulent shear stresses near the bottom of the plunge pool that break up the entrapped bubbles into finer particles (typically millimetric in size). This phenomenon resulted in a higher number of bubbles impacting on the optical fiber tip. The results show the characteristic profile reported by Chanson and Brattberg (2000) in free hydraulic jumps, which is a triangular profile in the turbulent

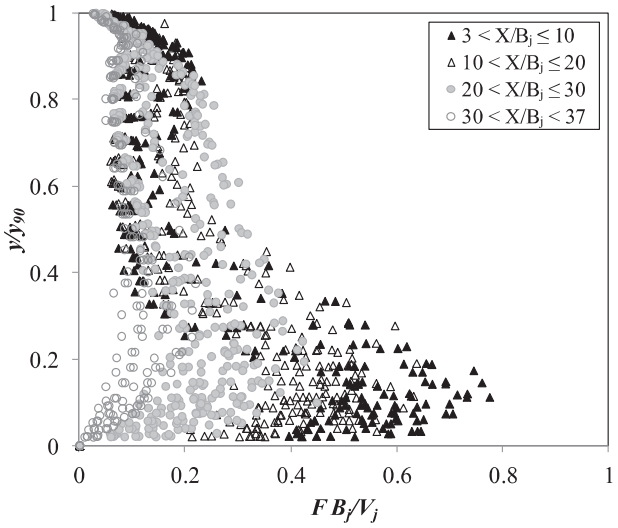

Fig. 7. Dimensionless change detection frequency profiles in the submerged hydraulic jump.

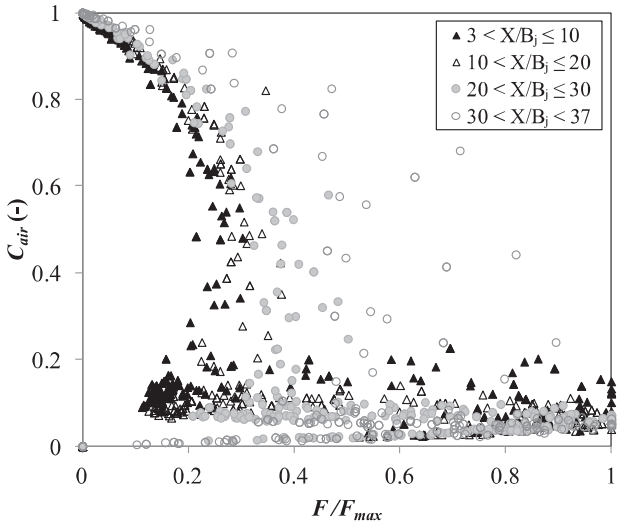

Fig. 8. Normalized frequency profiles as a function of the maximum frequency.

shear region, an abrupt change of slope at the upper edge of the shear region and a flatter shape in the re-circulation region.

The profiles closest to the beginning of the submerged hydraulic jump show a clear maximum peak around $0.10 < y/y_{90} < 0.30$, with the maximum reaching values of around 130-140 Hz for a X/B_j ratio between 3 and 10. The measured maximum frequency values were similar to those obtained by Murzyn and Chanson (2007), who measured maximum frequencies of around 120 Hz with a Froude number of 8.30 in free hydraulic jumps. The maximum frequency peak is related with the entrapped air in the plunge pool entered by the air-water turbulent jet that generates high irregularities around the impingement point (Ervine et al., 1980).

As the flow moves downstream, the maximum peak detected by the probe near the bottom tends to decrease. For $0.50 < y/y_{90} < 0.80$, the detected frequency tends to a constant value in almost all the distances (F between 10 and 50), with the maximum values for the cross sections located at X/B_j ratios between 20 and 30, while the closest sections to the stagnation point show the smallest values. Near the free surface ($y/y_{90} > 0.90$), the change phase frequency tends to reduce rapidly. This sharp reduction in frequency is consistent with the free surface undulation observed, which is associated with larger time scales.

Considering the C_{mean} values, the maximum peak observed near the bottom may be identified with the maximum values of C_{mean} observed in Fig. 4 (between 0.19 and 0.24). The maximum frequencies near the bottom tend to reduce as the C_{mean} in the vertical profiles reduces. In the intermediate part of the vertical profiles, the minimum frequencies tend to correspond with the minimum C_{mean} values (between 0.08 and 0.13), while the values registered in the other two sub-classes considered in Fig. 4 tend to be mixed.

The frequency profiles can also be analyzed if they are normalized as a function of the maximum frequency F_{max} obtained in each vertical profile (Fig. 8). Different regions are observed. The higher F/F_{max} values are obtained for low local concentration values ($C_{air} < 0.20$). Those points mainly correspond to the C_{air} and F peaks observed near the bottom in the previous figures. However, in cross sections with small C_{mean} values and/or located further away from the stagnation point, the range of frequencies in the vertical is smaller than near the impingement region.

For $0.20 < C_{air} < 0.80$, the F/F_{max} values are around 0.30 for $3 < X/B_j < 20$. However, the data are scattered in the profiles located further from the stagnation point. Near the free surface ($C_{air} > 0.80$), the F/F_{max} ratio tends to rapidly reduce to zero (larger time scales region).

3.4. Distribution of velocities in the dissipation basin

Using a modified Pitot tube corrected by the local void fraction with Eq. (5), the time-average velocity measurements were obtained in the same positions and conditions registered with the optical probe. This equipment enables the quasi-unidirectional flow in the wall jet of the submerged hydraulic jump to be analyzed. Near the bottom it may be considered that the streamlines are mainly parallel to the bottom, and the Pitot tube seems to be accurate at obtaining the horizontal mean velocity V_x. Outside the wall jet, the flow is not quasi-unidirectional and, according to Matos and Frizell (2000) and Matos et al. (2002), measurements may be affected by the angle of the velocity vector. For that reason, the velocities in the backwards region were not considered in the analysis.

Previous studies (e.g., Rajaratnam, 1965; Wu and Rajaratnam, 1995) have obtained that the vertical mean velocity profiles in the forward flow of free and submerged hydraulic jumps may be analyzed if they are normalized with a velocity scale equal to the maximum velocity V_{max} at any section, and with a length scale δ_l equal to the vertical distance y between the bottom and where the local velocity $V = V_{max}/2$. The velocity gradient is negative at this location.

Assuming this normalization, Castillo et al. (2017) proposed an adjustment formula based on physical and numerical measurements of a submerged hydraulic jump downstream of nappe jets with four specific flows between 0.023 and 0.082 $m^3/s/m$ for distances from the stagnation point that are greater than 0.4 m. De Dios et al. (2017) proposed a different adjustment for impingement Froude numbers between 3 and 5 for submerged hydraulic jumps generated downstream of a vertical sluice gate.

In this work, the length scale δ_1 and the maximum velocity V_{max} were obtained in each vertical profile of the five submerged hydraulic jumps. In the analyzed cases, the maximum mean velocities were obtained in the vicinity of the bottom in the cross sections located closest to the stagnation point, with maximum velocity values between 2.54 and 4.05 m/s.

Fig. 9 shows the normalized velocity profiles in the submerged hydraulic jump. Although the same sub-classes based on the X/B_j ratio have been considered in the figure, no remarkable behavior change was found among the data. The highest velocities were reg-

Table 4
Experimental adjustment proposed by several authors.

Authors	Experimental adjustment	Research	R^2
Rajaratnam (1976)	$\frac{V_x}{V_{max}} = e^{-0.693\left(\frac{y}{\delta_l}\right)^2}$	Plane turbulent free jet– nozzle	0.94
Lin et al. (2012)	$\frac{V_x}{V_{max}} = 2.3\left(\frac{y}{\delta_l}\right)^{0.42}\left(1 - erf\left(0.886\frac{y}{\delta_l}\right)\right)$	Free hydraulic jump– sluice gate	0.91
De Dios et al. (2017)	$\frac{V_x}{V_{max}} = 2.0\left(\frac{y}{\delta_l}\right)^{1/7}\left(1 - erf\left(0.55\frac{y}{\delta_l}\right)\right) - 0.39$	Submerged hydraulic jump– sluice gate	0.96
Castillo et al. (2017)	$\frac{V_x}{V_{max}} = 1.48\left(\frac{y}{\delta_l}\right)^{1/7}\left(1 - erf\left(0.66\frac{y}{\delta_l}\right)\right)$	Submerged hydraulic jump– nappe flow	0.97
New adjustment	$\frac{V_x}{V_{max}} = 1.70\left(\frac{y}{\delta_l}\right)^{0.11}\left(1 - erf\left(0.53\frac{y}{\delta_l}\right)\right) - 0.26$	Submerged hydraulic jump– nappe flow	0.98

where $erf(u) = \frac{2}{\sqrt{\pi}}\int_0^u e^{-t^2}dt$

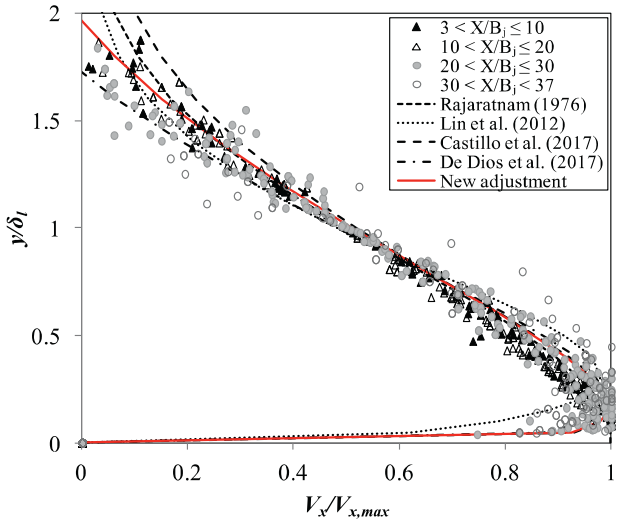

Fig. 9. Dimensionless profiles of horizontal mean velocity in the plunge pool.

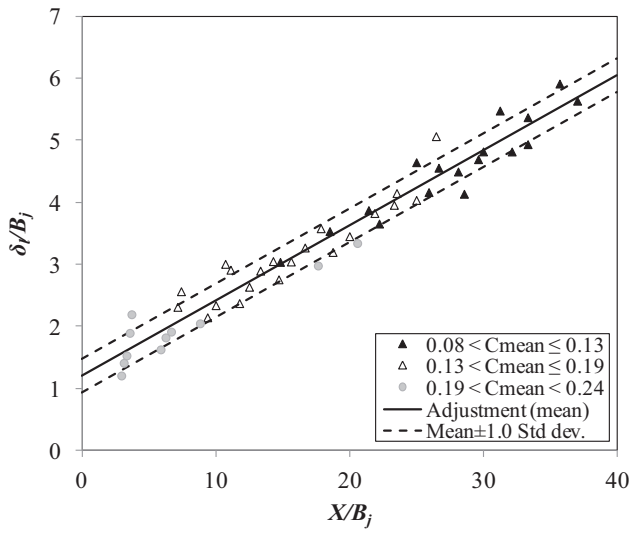

Fig. 10. Variation of the characteristic length scale in different sections of the submerged hydraulic jump.

istered close to the bottom. The mean velocity tends to decrease as the flow separates from the bottom. The registered values are also in agreement with the different dimensionless velocity distributions proposed by the studies listed in Table 4, as can be seen for their respective R^2 values for the current dataset. As reported by Long et al. (1990), the profiles of submerged hydraulic jumps are similar to those of a classical wall jet for y/δ_1 up to about 1.5. Beyond that, the $V_x/V_{x,max}$ profiles are mostly influenced by the reversing flow. The results also concur with the model proposed by Rajaratnam (1965), considering the submerged jump as a wall jet under an adverse pressure gradient.

The Rajarantam (1976) expression seems to follow the trend as the measurement points move from the bottom. However, this expression is unable to reproduce the expected velocity reduction for y/δ_1 ratios < 0.1. The Lin et al. (2012) expression was obtained for free hydraulic jumps and tends to obtain the maximum velocities slightly further away from the bottom wall than the other formulae. The empirical formulae obtained by Castillo et al. (2017) and De Dios et al. (2017) show similar behavior for y/δ_1 ratios < 1. A new dimensionless adjustment has been proposed, slightly improving previous adjustments. Although the inlet flow conditions were different, the results indicate that the velocity distribution near the bottom of submerged hydraulic jumps downstream of rectangular free falling jets may be described with relative good agreement with those formulae obtained in different flow conditions.

Following Long et al. (1990), the characteristic length δ_l along the submerged hydraulic jumps can be considered for analyzing the velocity scale decay in submerged jumps. Fig. 10 shows the length scale values in a dimensionless way for the impingement jet thickness B_j. Data have been plotted considering the previous sub-classes of the mean void fraction in the vertical profiles.

The behavior is similar to that observed by Wu and Rajaratnam (1995) in wall jets, with data tending to fall within one standard deviation of the mean value. Considering the results obtained in this type of submerged hydraulic jump downstream of a nappe jet, an adjustment can be obtained with $R^2 = 0.95$, independently of the C_{mean} value:

$$\frac{\delta_l}{B_j} = 0.121\frac{X}{B_j} + 1.205 \tag{9}$$

The slope is similar to those of the results reported by different authors. For instance, Rajaratnam and Humphries (1984) obtained a slope of 0.07 in plane surface jets; Long et al. (1990) considered that submerged jumps may be treated as wall jets under an adverse pressure gradient. Wu and Rajaratnam (1995) observed that the free jumps grow at about the same rate as that of the wall jet (slope of 0.0728) in the early stage but grow faster later on. In addition, most of the observations for submerged jumps are contained within one standard deviation of the wall jet, while the data near the end of the jump show an accelerated growth rate; Raiford and Khan (2009) observed that the growth rate in circular jets for low submergences was 0.071 for $x/d = 24 - 35$, and 0.13 – 0.17 for further sections, with d being the nozzle diameter.

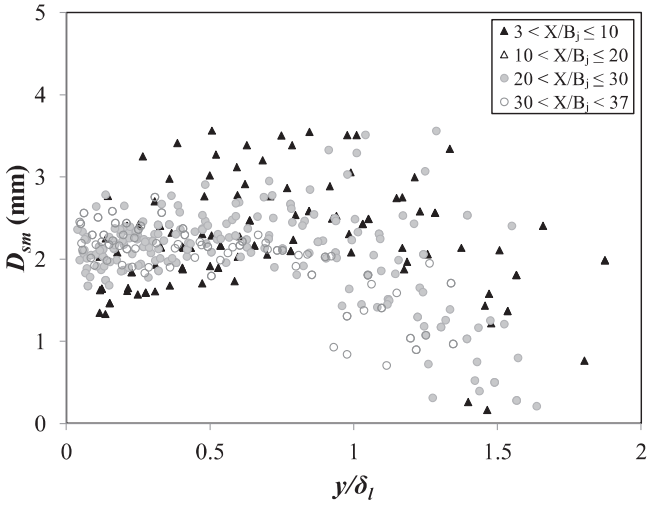

Fig. 11. Sauter mean bubble diameter in the submerged hydraulic jump.

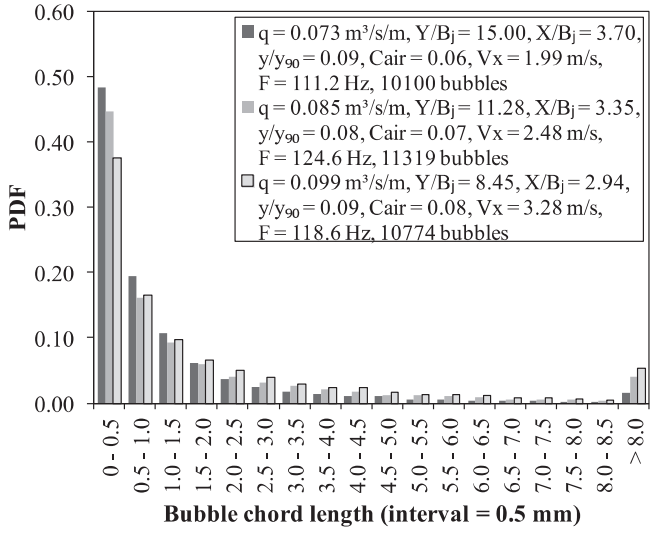

Fig. 12. Probability distribution function (PDF) of the bubble chord length at $X = 0.10$ m downstream of the stagnation point.

3.5. Mean bubble size

Assuming that the time-average velocity presented in the previous section is right, and taking into account the simplifications that the bubbles can be considered to be spherical in shape, equally distributed in time and that their movement is one-directional, the mean bubble diameter may be obtained by the Sauter mean bubble diameter D_{sm} (Clift et al., 1978; RBI-Instrumentation, 2012). This is the mean bubble diameter whose volume/surface ratio is the same as that calculated for all the bubbles detected during each measurement. The Sauter mean bubble diameter can be defined as:

$$D_{sm} = \frac{3C_{air}V}{2F} \tag{10}$$

where C_{air} is the void fraction, V the mean velocity of the bubbles obtained with Eq. (5) (assuming the bubbles have the same velocity as the flow), and F the change phase detection frequency.

Fig. 11 shows the Sauter mean bubble diameter obtained in the plunge pool. The new adjustment of dimensionless velocity distribution has also been plotted. As the validity of the velocity field was limited to the wall jet region, the upper part of the vertical profiles has been discarded. The diameters are mostly around 2 mm, with maximum values below 4 mm. Once the distance to the bottom is larger than the characteristic length scale of the submerged hydraulic jump ($y > \delta_l$), the data seem to show a scattered behavior with a reduction in the Sauter mean bubble diameter. Scattered data are generally those data obtained in cross sections located further away from the stagnation point and with less air concentration. The profiles with the larger values of C_{mean}, hence those closest to the stagnation point, obtain a more varied range of Sauter mean bubble diameter, including many of the largest D_{sm} values, while the minimum values of D_{sm} are mainly obtained in cross sections with the larger X/B_j ratio values. These diameters concur with those obtained by Carrillo et al. (2020a) using a combination of experimental and numerical techniques.

The phase change size may be classified as a function of the bubble chord length distributions, obtained as the time the optical probe tip is in air multiplied by the local mean velocity (e.g., Chanson, 2007; Chanson and Chachereau, 2013). Using the velocity field validated in the previous section, Fig. 12 shows the probability of finding each bubble chord length in the first section measured in the wall jet (located at $X = 0.10$ m), located at the same dimensionless distance from the bottom ($y/y_{90} = 0.08$-0.09), for the maximum, intermediate and minimum specific flows. Similar values were obtained for different dimensional (frequency, number of detected bubbles) and dimensionless (X/B_j, y/y_{90} and C_{air}) parameters. In turn, the choice of those points allows the influence of the effective tailwater rate Y/B_j (from 8.45 to 15.00) to be analyzed. Considering the plotted results, the trend of the bubble chord length distribution seems to be independent of the Y/B_j value. In all the cases, the probability distribution function (PDF) tends to be higher for bubble chord lengths between 0 and 0.5 mm. The data with the smaller flow velocity obtain a relatively larger maximum PDF value. As the bubble chord length increases, a right-skewed distribution is observed as the probability of finding each sub-interval tends to reduce drastically. As several researchers have stated in their description of punctual phase change probes, this PDF distribution with the maximum in the smaller interval may be related with the difficulty of puncturing the bubbles on their exact central axis. Furthermore, larger bubbles tend to an ellipsoidal shape, becoming more distorted and less spherical in shape with increasing size (Harmathy, 1960).

In the three cases considered, around 71-85% of the bubble chord lengths are smaller than 2 mm, and around 85-94% are smaller than 4 mm, with those percentages being higher as the local flow velocity of the tested point is smaller. Those results are also in agreement with the Sauter mean bubble diameter observed in Fig. 11.

4. Conclusions

The study of two-phase air-water flows is a challenge in hydraulic structures due to the undiluted mixture of the flow.

In the present study, the characteristics of the air-water flow of five submerged hydraulic jumps generated downstream of nappe jets have been analyzed. The equipment (optical fiber probe and modified Pitot tube) was used considering their limitations. Hence, the velocity measurements were limited to the wall jet region.

The distance from the stagnation point to the impingement jet thickness ratio X/B_j and the mean void fraction in the vertical profile C_{mean} seem to be good dimensionless parameters for identifying different behaviors of the void fraction distribution in vertical profiles. However, the dimensionless velocity profiles seem to be independent of those classifications.

Near the bottom, the local peaks of void fraction and phase detection frequency were obtained close to the stagnation point of the rectangular jet, reaching void fraction values around 20-25% and with a frequency around 130-140 Hz. For analyzing the

local void fraction peak, a formula proposed for free hydraulic jumps was adapted with a suitable fit.

The void fraction and the frequency local peaks tend to decrease as the flow moves downstream from the impingement region. Near the free surface, the local void fraction increases rapidly due to the undulation observed in the free surface of the plunge pool. However, the phase change frequency tends to minimum values in all the measured cross sections. The phase change frequency behavior is similar to those reported by several authors in free hydraulic jumps (e.g., Chanson and Brattberg, 2000; Murzyn et al., 2005).

The normalized velocities follow the behavior observed in free hydraulic jumps, with the maximum velocities being in the wall jet region. Our finding extends the validity range of previous studies performed by several researchers (e.g., Castillo et al., 2017; De Dios et al., 2017) in the field of submerged hydraulic jumps. The velocities tend to decrease as the flow exits from the shear layer. Dimensionless velocity adjustments were proposed for the mean velocity and the growth of the shear layer for submerged hydraulic jumps generated downstream of rectangular free falling jets, with $R^2 = 0.98$ and 0.95, respectively.

The bubble chord length distributions showed a higher probability for values of bubble chord length between 0 and 0.5 mm near the stagnation point, independently of the Y/B_j ratio.

Data on air entrapped and velocity field downstream of nappe jets are scarce. Although in this type of jets the flow enters almost vertically, in general the formulae previously published in free hydraulic jumps and submerged hydraulic jumps downstream of a gate may be used and/or adapted for submerged hydraulic jump downstream of nappe jets. This allows to consider that our results may be representative of this type of flow conditions.

Declaration of Competing Interest

The authors declare that they have no known competing financial interests or personal relationships that could have appeared to influence the work reported in this paper.

CRediT authorship contribution statement

José M. Carrillo: Conceptualization, Methodology, Validation, Formal analysis, Writing - original draft, Writing - review & editing, Resources, Supervision, Funding acquisition. **Francisca Marco:** Investigation, Formal analysis, Visualization. **Luis G. Castillo:** Conceptualization, Methodology, Validation, Resources, Visualization, Supervision, Writing - review & editing, Funding acquisition. **Juan T. García:** Conceptualization, Writing - review & editing, Supervision.

Acknowledgments

The researchers express their gratitude for the financial aid received from the "Ministerio de Ciencia, Innovación y Universidades" (MCIU), the "Agencia Estatal de Investigación" (AEI) and the "Fondo Europeo de Desarrollo Regional" (FEDER), through the Project “La aireación del flujo en el vertido en lámina libre por coronación de presas a nivel de prototipo y su efecto en cuencos de disipación de energía”, Ref: RTI2018-095199-B-I00.

The work was partially funded by the "Comunidad Autónoma de la Región de Murcia" through the "Programa Regional de Fomento de la Investigación Científica y Técnica (Plan de Actuación 2018) de la Fundación Séneca-Agencia de Ciencia y Tecnología de la Región de Murcia”, Project “Análisis de la capacidad de descarga de vertederos tipo laberinto y de la disipación de energía aguas abajo de los mismos”, Ref: 20879/PI/18.

The second author thanks the Ministerio de Educación, Cultura y Deporte for the financial aid received from the University Teacher Training Grant (FPU), reference number FPU16 / 05658.

References

Albertson, M.L., Dai, Y.B., Jenson, R.A., Rouse, H., 1950. Diffusion of submerged jets. Procs. ASCE, p. 74.

André, S., Boillat, J.L., Schleiss, A.J., 2005. Discussion of ‘Two-phase flow characteristics of stepped spillways’ by Robert M. Boes and Willi H. Hager. Journal of Hydraulic Engineering 131 (5), 423–427.

Annandale, G.W., 2006. Scour technology. Mechanics and Engineering Practice. McGraw-Hill, New York.

Bertola, N., Wang, H., Chanson, H, 2018. A physical study of air–water flow in planar plunging water jet with large inflow distance. International Journal of Multiphase Flow 100, 155–171.

Bollaert, E.F.R., Schleiss, A.J, 2003. Scour of rock due to the impact of plunging high velocity jets, Part 2: experimental results of dynamic pressures at pool bottoms and in one- and two- dimensional closed end rock joints. J Hydraul Res 41 (5), 465–480.

Boes, R., Hager, W.H., 1998. Fiber-optical experimentation in two-phase cascade flow. In: HANSEN, K. (Ed.), Proc. Int. RCC Dams Seminar. Denver, USA Editor.

Boes, R., Hager, W.H., 2003. Two-phase flow characteristics of stepped spillways. Journal of Hydraulic Engineering 129 (9), 661–670.

Carrillo, J.M., 2014. Metodología numérica y experimental para el diseño de los cuencos de disipación en el sobrevertido de presas de fábrica. PhD Thesis. Universidad Politécnica de Cartagena.

Carrillo, J.M., Matos, J., Lopes, R., 2019. Numerical modeling of free and submerged labyrinth weir flow for a large sidewall angle. Environmental Fluid Mechanics 20, 357–374.

Carrillo, J.M., Castillo, L.G., Marco, F., García, J.T., 2020a. Experimental and numerical analysis of two-phase flows in plunge pools. *Journal of Hydraulic Engineering*, ASCE 146 (6). doi:10.1061/(ASCE)HY.1943-7900.0001763.

Carrillo, J.M., Marco, F., Castillo, L.G., García, J.T., 2020b. Analysis of two-phase flows in plunge pools of nappe jets. In: Proc., 8th IAHR International Symposium on Hydraulic Structures, Santiago de Chile, Chile, pp. 12–15.

Castillo, L.G., 2006. Aerated jets and pressure fluctuation in plunge pools. In: *Proc., of the Seventh International Conference on Hydroscience and Engineering* 2006, Philadelphia. M. Piasecki and College of Engineering, Drexel University, USA, pp. 1–23.

Castillo, L.G., Carrillo, J.M., Blázquez, A., 2015. Plunge pool mean dynamic pressures: a temporal analysis in nappe flow case. Journal of Hydraulic Research 53 (1), 101–118.

Castillo, L.G., Carrillo, J.M., Bombardelli, F.A., 2017. Distribution of mean flow and turbulence statistics in plunge pools. Journal of Hydroinformatics 19 (2), 173–190.

Castillo, L.G., Carrillo, J.M., Sordo-Ward, A., 2014. Simulation of overflow nappe impingement jets. Journal of Hydroinformatics 16 (4), 922–940.

Chachereau, Y., Chanson, H, 2011. Bubbly flow measurements in hydraulic jumps with small inflow Froude numbers. International Journal of Multiphase Flow 37, 555–564.

Chanson, H., 1995. Air entrainment in two dimensional turbulent shear flows with partially-developed inflow conditions. International Journal of Multiphase Flow 21 (6), 1107–1121.

Chanson, H., 2007. Bubbly flow structure in hydraulic jump. European Journal of Mechanics B/Fluids 26, 367–384.

Chanson, H., 2009. Turbulent air-water flows in hydraulic structures: dynamic similarity and scale effects. Environ Fluid Mech 9, 125–142.

Chanson, H., Aoki, S., Hoque, A., 2004. Physical modelling and similitude of air bubble entrainment at vertical circular plunging jets. Chemical Engineering Science 59, 747–758.

Chanson, H., Brattberg, T., 2000. Turbulent experimental study of the air-water shear flow in a hydraulic jump. International Journal of Multiphase Flow 26 (4), 583–607.

Chanson, H., Chachereau, Y., 2013. Scale effects affecting two-phase flow properties in hydraulic jump with small inflow Froude number. Experimental Thermal and Fluid Science 45, 234–242.

Clift, R., Grace, J.R., Weber, M.E., 1978. Bubbles, drops and particles. Academic Press, New York.

De Dios, M., Bombardelli, F.A., García, C.M., Liscia, S.O., Lopardo, R.A., Parravicini, J.A., 2017. Experimental characterization of three-dimensional flow vertical structures in submerged hydraulic jumps. Journal of Hydro-environment Research 15, 1–12.

Duarte, R., Schleiss, A.J., Pinheiro, A., 2015. Optical fibre probe measurements of bubble flow in hydraulic jumps. Environ Fluid Mech 15, 673–693. doi:10.1007/s10652-014-9392-x.

Ervine, D.A., 1998. Air entrainment in hydraulic structures: a review. Proc. Instn Civ. Engrs Wat., Marit. & Energy 130 (3). doi:10.1680/iwtme.1998.30973, Sept., 142–153.

Ervine, D.A., Falvey, H.T., 1987. Behavior of turbulent eater jets in the atmosphere and in plunge pools. Proceedings of the Institutions of Civil Engineers 83 (2), 295–314.

Ervine, D.A., Falvey, H.T., Withers, W., 1997. Pressure fluctuations on plunge pool floors. Journal of Hydraulic Research 35 (2), 257–279.

Ervine, D.A., Mckeogh, E.J., Elsawy, E.M., 1980. Effect of turbulence intensity on the rate of air entrainment by plunging water jets. Proc Instn Civ Engrs 69, 425–445 Part 2 June.
FEMA, 2013. Selecting and accommodating inflow design floods for dams. US Department of Homeland Security, USA Federal Emergency Management Agency. FEMA P-94.
FEMA, 2014. Technical manual: Overtopping protection for dams. Federal Emergency Management Agency. FEMA P-1014. US Department of Homeland Security, USA.
Harmathy, T.Z., 1960. Velocity of Large Drops and Bubbles in Media of Infinite or Restricted Extent. AIChE Journal 6, 281–288.
Horeni, P. (1956). Disintegration of a free jet of water in air. Vyzkumny Ustav Vodohospodarsky Prace a Studie, *Sesit* 93. Prague, Czechoslovakia, (in Czech).
Lin, C., Hsieh, S.C., Lin, I.J., Chang, K.-A., Raikar, R.V., 2012. Flow property and self-similarity in steady hydraulic jumps. J. Exp. Fluids 53, 1591–1616.
Long, D., Steffler, P.M., Rajaratnam, N., 1990. LDA study of flow structure in submerged hydraulic jump. Journal of Hydraulic Research 28 (4), 437–460.
Long, D., Steffler, P.M., Rajaratnam, N., 1991. A numerical study of submerged hydraulic jumps. Journal of Hydraulic Research 29 (3), 293–308.
Lopes, R., 2011. Capacidade de vazão, energia específica residual e caracterização do escoamento de emulsão ar-água em soleiras descarregadoras em labirinto. Ph.D. Thesis. Instituto Superior Técnico, Universidade Técnica de Lisboa.
Manso, P.A., Bollaert, E.F.R., Schleiss, A.J, 2007. Impact pressures of turbulent high-velocity jets plunging in pools with flat bottom. Exp Fluids 42, 49–60.
Matos, J., Frizell, K.H., André, S., Frizell, K.W., 2002. On the performance of velocity measurement techniques in air-water flows. In: Proceedings of the Hydraulic Measurements and Experimental Methods Conference. Estes Park, USA. EWRI/ASCE & IAHR.
Matos, J., Frizell, K.H., 2000. Air concentration and velocity measurements on self-aerated flow down stepped chutes. In: Proc., 2000 Joint Conf. on Water Resources Engineering and Water Resources Planning & Management. Minneapolis, USA. ASCE.
Murzyn, F., 2010. Assessment of different experimental techniques to investigate the hydraulic jump: do they lead to the same results? In: Proc., 3rd International Junior Researcher and Engineer Workshop on Hydraulic Structures, Edinburg, UK, pp. 3–36 May 02-04.
Murzyn, F., and Chanson, H. (2007). Free surface, bubbly flow and turbulence measurements in hydraulic jumps, Report N°CH63/07, Division of Civil Engineering, The University of Queensland, Brisbane, Australia.
Murzyn, F., Chanson, H., 2009. Free-surface fluctuations in hydraulic jumps: experimental observations. Experimental Thermal and Fluid Science 33 (7), 1055–1064.
Murzyn, F., Mouaze, D., Chaplin, J.R., 2005. Optical fibre probe measurements of bubble flow in hydraulic jumps. International Journal of Multiphase Flow 31, 141–154.
Peiqing, L., Jizhang, G., Yongmei, L., 1998. Experimental investigation of submerged impinging jets in a plunge pool downstream of large dams. Science in China (Series E) 41 (4), 357–365.
Raiford, J.P., Khan, A.A., 2009. Investigation of circular jets in shallow water. Journal of Hydraulic Research 47 (5), 611–618.
Rajaratnam, N., 1965. The hydraulic jump as wall jet. Proc. ASCE J. Hydraul. Div. 91 (HY5), 107–132.
Rajaratnam, N., 1976. Turbulent Jets, 5. Elsevier Scientific, Development in Water Science, New York, USA.
Rajaratnam, N., Humphries, J.A., 1984. Turbulent non-buoyant surface jets. Journal of Hydraulic Research 22 (2), 103–115.
Ranga Raju, K.G., Asawa, G.L., 1977. Viscosity and surface tension effects on weir flow. Journal of the Hydraulics Division 103 (10), 1227–1231.
RBI-Instrumentation (2012). ISO Software user's guide.
Scimemi, E., 1930. Sulla Forma delle Vene Tracimanti. L'Energia Elettrica 7 (4), 293–305 (in Italian).
Stutz, B., 1996. Analyse de la structure diphasique et instationnaire de poches de cavitation PhD Thesis. Institut National Polytechnique de Grenoble.
Stutz, B., Reboud, J.L., 1997a. Experiment on unsteady cavitation. Experiments in Fluids 22, 191–198.
Stutz, B., Reboud, J.L., 1997b. Two-phase flow structure of sheet cavitation. Physics of Fluids 9 (12), 3678–3686.
Valero, D., Viti, N., Gualtieri, C., 2018. Numerical Simulation of Hydraulic Jumps. Part 1: Experimental Data for Modelling Performance Assessment. Water 11 (36), 1–16.
Wood, I.R., 1983. Uniform region of self-aerated flow. *Journal of Hydraulic Div*., ASCE 109 (3), 447–461.
Wood, I.R., 1991. Air entrainment in free-surface flows. IAHR ISBN: 90-6191-994-0.
Wu, S., Rajaratnam, N., 1995. Free jumps, submerged jumps and wall jets. Journal of Hydraulic Research 33, 197–212. doi:10.1080/00221689509498670.
Xu, W., Chen, C., Wei, W., 2018. Experimental Study on the Air Concentration Distribution of Aerated Jet Flows in a Plunge Pool. Water 10, 1779 2018.